PC4199 HONOURS PROJECT IN PHYSICS

X-Ray Absorption Spectroscopy
And
Modelling of scattering factors of condensed matter

Ang Wee Pin

A0140453R

Supervisor:

Associate Professor Andrivo Rusydi

An academic exercise submitted to the Department of Physics

National University of Singapore

in partial fulfilment for the degree of

Bachelor of Science (Honours) in Physics

Academic Year 2018/2019

TABLE OF CONTENTS

ACKNOWLEDGEMENTS

I would like to thank Professor Andrivo for accepting my request to be my supervisor for my Final Year Project. Professor Andrivo is always smiling and laughing when I approach him for queries in his office. He makes discussions really enjoyable and stress-free. Despite my lack of understanding in the topic, Prof Andrivo never once got frustrated trying to explain concepts and theories to me, but instead he suggested topics for me to self-research on and he gave me a lot of freedom when it comes to the pace of research.

My commitments in TeamNUS climbing as the captain this AY has made my final two semesters in NUS super busy and as such I was not able to meet Prof Andrivo as often. However, he would gladly offer to meet on Skype for discussion, saying that we should make full use of technology. I remembered being so busy with an event earlier this January but I still ended up meeting him over Skype past office hours at 10pm. For that, I am very grateful and thankful to have a supervisor like Prof Andrivo who gives me so much flexibility in my research despite my busy schedule.

ABSTRACT

The discovery of X-rays in 1895 by Wilhelm Conrad Roentgen led to a series of research on the topic. X-ray emission spectroscopy was pioneered by the Braggs who realised that interatomic spacing are close to the wavelength of X-rays. The nature of the properties of X-ray allowed for the study of materials in the atomic scale.

X-ray absorption spectroscopy is widely used in fields such as molecular physics and material science. X-ray absorption spectroscopy can be categorised based on the incident photon energy such as X-ray Absorption Near Edge Structure and Extended X-ray Absorption Fine Structure. The differences in the applications and theories behind these categories are being explained in Chapter 1.

At the start of the project, a graph of X-ray refractive index (delta and beta) being plotted against photon energy was presented to me by my supervisor. The graph is generated from an online X-ray database provided by The Centre for X-ray Optics, a multi-disciplined research group based in Lawrence Berkeley National Laboratory's Materials Sciences Division. The main part of the study is to understand how the graph was being generated and the algorithms behind it. It was found that the values of delta and beta of a condensed matter can be calculated from its scattering factor; which is approximated by summing up the atomic scattering factors of individual elements present in the compound.

LIST OF FIGURES AND TABLES

INTRODUCTION

1.1 History of X-rays

The discovery of X-rays in 1895 by Wilhelm Conrad Roentgen, a German physicist, was a remarkable stepping stone in the history of Science; especially in the field of Physics. After the discovery of X-rays, many scientists researched on the use of it. William Lawrence Bragg and William Henry Bragg were two of the many scientists. They were a team of father and son who researched on X-raysand won the Nobel Prize in 1915 “for their services in the analysis of crystal structure by means of X-rays.”

Their works were possible due to the fact that the wavelengths of X-rays were of similar order as the separation of the atoms in crystalline materials. X-ray diffraction was one of Lawrence’s significant works and it led to the famous Bragg’s diffraction law (Eq. 1).

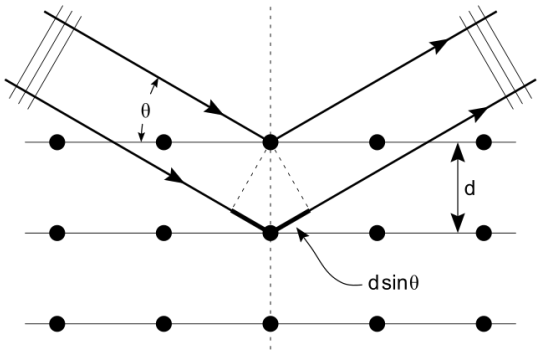

Figure1.1 Bragg's diffraction

$$n\lambda = dsin\theta \quad (1)$$

Bragg’s diffraction law (Eq. 1) showed that it was possible to find out the spacing between the sheets of atoms in a crystalline structure as long as the incident angle of X-ray and the wavelength of the X-ray are specified. By knowing the spacing between the sheets of atoms in a crystalline structure, many analyses could be done on different crystals. Since then, X-ray spectroscopy has been widely used for the characterization of materials and it had been categorised into different branches mainly X-ray Emission Spectroscopy (XES) and X-Ray Absorption Spectroscopy (XAS).

1.2 X-ray emission spectroscopy (XES)

William Lawrence Bragg and William Henry Bragg were both considered to be the original pioneer of XES. In XES, high energy particles such as electrons bombard the crystal of interest. The core electrons of the atom get excited to a higher level. When the electrons relax and undergo fluorescence, it emits electromagnetic radiation in the X-ray regime. Since the energy difference in different energy levels are specific to different

elements, the wavelength of the X-rays that are emitted are specific. This allows for XES to be a method used to determine the element present in a material and its specific electronic configuration.

XES can be further split into Resonant XES (RXES) and Non-resonant XES (NXES). The difference between RXES and NXES is the way in which the atom is excited. For RXES, the atoms undergo resonant excitation while in NXES, the atoms undergo non-resonant excitation.

Resonant excitation occurs when the incoming photon energy corresponds to the energy required to excite a core electron into an unoccupied valence state. In RXES, if the initial electronic configuration and the final electronic configuration after fluorescence are the same, which means that the incident and emitted photon energy is the same, this form of RXES is called resonant elastic x-ray scattering. For RXES that have differing incident and emitted photon energy, it is called resonant inelastic x-ray scattering (RIXS).

Non-resonant excitation occurs in NXES where incident photons do not correspond to the energy needed to promote a core electron to an unoccupied valence state. The difference in the energy between the incident photon and emitted photon can be studied to analyse the electronic configuration of the sample.

1.3 Difference between XES and XAS

XAS works in a similar way to XES where high energy photons bombard a given sample. The main difference is that XAS probes the absorption energy when core electrons gets excited into higher energy levels while the XES probes the emission energy when electrons in the higher energy levels relax and decay into lower energy levels. In this way, XAS probes the unoccupied density of electronic states of a material while XES probes the occupied density of electronic states of a material. Hence, XES and XAS works as complements to understand the full electronic configuration of a given sample.

For XAS, the energy of incoming photons is tunable over a wide range and the absorption coefficients of the sample at different photon energy are measured. The relationship between the absorption coefficient and

incoming photon energy can be analysed and it will determine the local electronic and structural properties of the sample.

For XES, specifically RXES, the incoming photon energy are set to be well above the absorption edges. XES measures the energy of the photons emitted by the sample during fluorescence and hence, determining the electronic structure of the sample.

1.4 Incident photon sources – Synchrotron Radiation Facilities

XAS requires high intensity and tunable X-rays. XAS are usually conducted in synchrotron radiation facilities where synchrotron light sources that are of the order of GeVs are created. These synchrotron radiation facilities are circular and usually have large circumference.

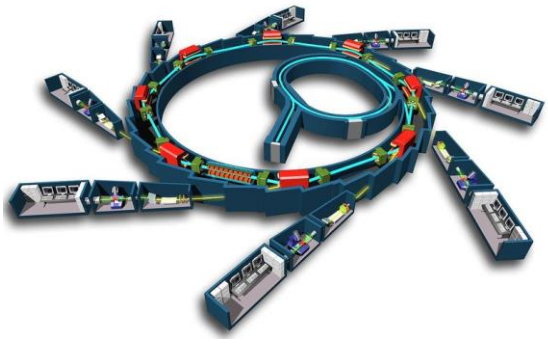

Figure 1.2 Soliel, a synchrotron radiation facility in Paris.

The Soliel is a synchrotron facility located near Paris. It has a circumference of 354m. The large circumference is needed for electrons to accelerate to near the speed of light. In the core of the synchrotron, electrons are emitted from an electron gun, a device which works very similar to cathode ray tubes found in old televisions. The electrons are then accelerated by a series of strong magnets in circular orbits in the first ring (the smaller ring in Fig 1.2). The first ring (also called the booster ring) is where the electrons are accelerated to near the speed of light by alternating magnetic fields. These high energy electrons are then pumped into the second ring (the larger ring in Fig 1.2). This second ring is also called the storage ring. The storage ring consists of powerful bending magnets which changes the direction of the highly energised electrons. Synchrotron light sources are produced when these high energy electrons change direction, emitting powerful X-rays into beam lines that are used in XAS. There are several synchrotron radiation facilities available in all parts of the world. These facilities usually produce high intensity radiation with energy in the GeVs. The energy of the radiation produced by synchrotron facilities are tunable using crystalline

monochromator for different experimental purpose such as XAS.

1.5 Introduction of XAS

XAS is being used in many different fields such as molecular physics and material science. It is usually done in synchrotron radiation facilities where incident photon energies are intense and tunable at narrow energy resolution. Due to the highly penetrating X-rays produced by synchrotron light sources, the samples of XAS can be solid, liquid or gaseous. The spectra are usually produced in a graph of absorption against incident photon energy. The absorption of x-ray by the sample is calculated by subtracting the emitted photon energy from the incident photon energy.

XAS is unique as compared to methods like XES and X-ray Diffraction (XRD) as it provides a way to look into the local geometrical structure of materials which is explained in section 1.7. The study of X-ray Absorption Spectroscopy (XAS) can be classified into 2 general categories namely X-ray Absorption Near Edge Structure (XANES) and Extended X-ray Absorption Fine Structure (EXAFS).

1.6 XANES

As inferred from the name, XANES deals with absorption spectra near the absorption edge. The absorption edge refers to the sharp increase in absorption when the incident photon energy corresponds to the binding energy of the core electrons.

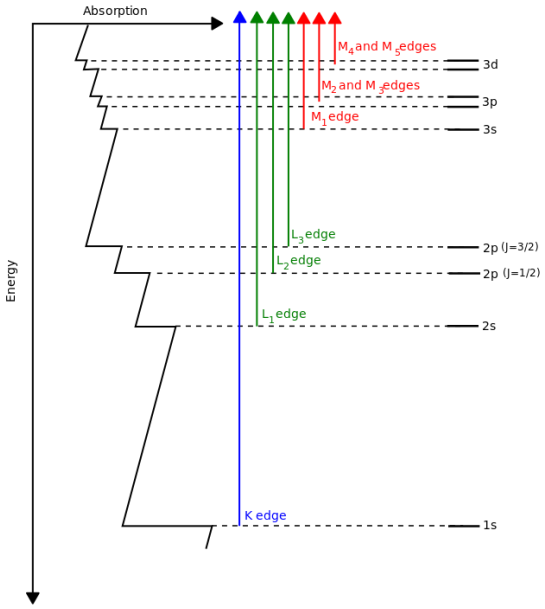

Figure 1.3 An illustration of the absorption spectrum of a metal atom. The different edges refer to the excitation of electrons from different electron orbitals.

NAXES spectra can be further split into two categories namely K-edge and L-edge spectroscopy. K-edge and L-edge spectroscopy are two NAXES categories that refer to the studies of electronic structures of transition metals by means of probing x-ray absorption near absorption edge. Metal K-edge spectroscopy zooms in to the absorption spectrum when a 1s electron is excited to a valence state while Metal L-edge spectroscopy

zooms in to the absorption spectrum when 2p or 2s electron isexcited to avalence state.

As seen in Fig 1.3, L edge can be split into 3 different edges, L1, L2 and L3. L1 edge deals with the binding energy of electrons in the 2s orbital while L2 and L3 deals with the binding energy of electrons in the $2P_{1/2}$ and $2P_{3/2}$ orbitals. The splitting of the 2p orbital is due to the spin-orbit interaction. The ability to measure and differentiate the L2 and L3 edges shows that XANES is able to distinguish different electron spins of the element in the sample.

XANES is element specific as different elements have different core level binding energy. Also, because XANES can measure the absorption of the transitions of core electrons to valence bound states, it can probe the unoccupied band structure of a material.Spectra with incident energy above the rising edge are categorised into EXAFS. Fig 1.4 shows a schematic of where XANES and EXAFS stand on the absorption spectra.

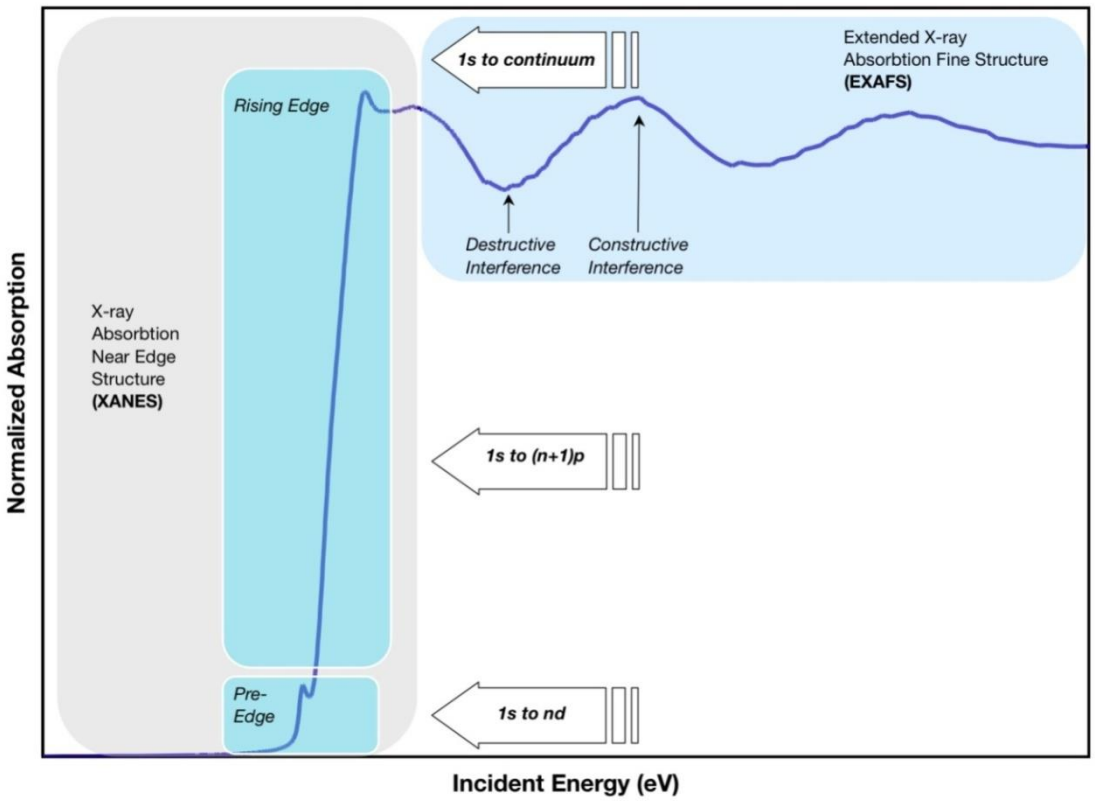

Figure 1.4 X-ray Absorption Spectra showing the range where XANES and EXAFS stand

1.7 Local geometric study using EXAFS

EXAFS spectra as mentioned earlier, has the ability to look into the local geometric of the sample. EXAFS analyses the X-ray absorption coefficient of a sample against incident photon energy at energy levels after the rising absorption edge. The uniqueness of EXAFS lies in the ability to measure interatomic distance.

Fig 1.4 shows a trough and a crest that is present in the EXAFS spectrum. The trough represents destructive interference while the crest represents constructive interference. These interferences occur because at energy levels higher than the absorption edge, there are 'left-over' energy that produces photoelectrons. These photoelectrons have de Broglie wavelength which is given in (Eq. 2)

$$\lambda_e = \frac{h}{p_e} \qquad (2)$$

where λ_e is the de Broglie wave, h is the planck's constant and p_e is the momentum of the photoelectron.

$$E_e = \frac{{p_e}^2}{2m_e} \qquad (3)$$

(Eq. 3) shows the kinetic energy equation where E_e is the energy of the photoelectron and m_e is the mass of the photoelectron. Putting (Eq. 2) and (Eq. 3) together, the de Broglie wavelength of the photoelectron is found to be (Eq. 4)

$$\lambda_e = \frac{h}{\sqrt{2m_e E_e}} = \frac{h}{\sqrt{2m_e(E - E_0)}} \qquad (4)$$

where E is the incident photon energy and E_0 is the binding energy of the edge.

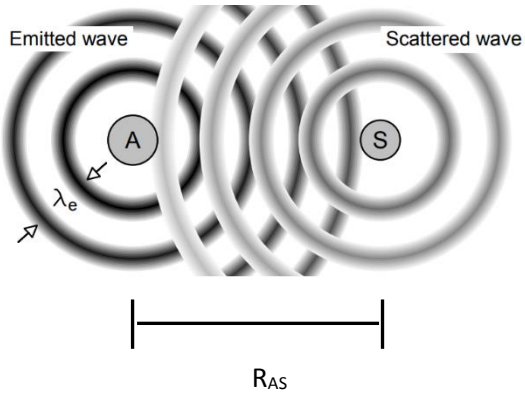

Figure 1.5 Interference between absorbing atom and scattering atom. Denote distance between the two atoms as R_{AS}.

The interferences occur due to the wave interactions between ejected photoelectron and the electrons of neighbouring atoms. In Fig 1.5, 'A' represents the absorbing atom which produces the photoelectron and 'S' represents the scattering atom which is also the neighbouring atom.

The absorbing atom emits wave of λ_e. As seen in Fig 1.5, the photoelectron wave emitted by the absorbing atom will be back scattered by the neighbouring atom. When the photoelectron wave travels from 'A' to 'S' and then from 'S' to 'A' when it gets deflected, there is a change in phase of Δ_{phase} (Eq. 5).

$$\Delta_{phase} = 2\pi\left(\frac{2R_{AS}}{\lambda_e}\right) \qquad (5)$$

where R_{AS} is the distance between the absorbing atom and the scattering atom.

During destructive interference, the back scattered waves and the emitted waves are completely out of phase; Δ_{phase} is 180° or more specifically (2n-1) π where n is an integer 1,2,3…

During constructive interference, the back scattered waves and the emitted waves are completely in phase;Δ_{phase} is 360° or more specifically 2nπ where n is an integer 1,2,3…

Hence, if we were to measure the incident energy E (Fig 1.4) where the destructive and constructive interference occur and using n = 1 for the first destructive interference and constructive interference, we get the following equations (Eq. 6) and (Eq. 7)

$First\ destructive\ inteference\ (n = 1)$

$$R_{AS} = \frac{\lambda_e}{4} = \frac{h}{4\sqrt{2m_e(E - E_0)}} \qquad (6)$$

$First\ constructive\ inteference\ (n = 1)$

$$R_{AS} = \frac{\lambda_e}{2} = \frac{h}{2\sqrt{2m_e(E - E_0)}} \qquad (7)$$

From (Eq.6) and (Eq. 7), we are able to determine the interatomic distance between the absorbing atom and scattering atom. Hence, showing the ability of EXAFS to analyse and measure local geometric of the sample.

However, it is to note that (Eq.6) and (Eq. 7) are derived with a simplified model of single scattering. Also, when the waves travel from 'A' to 'S', the varying in potential between the two atoms will lead to changes in the overall phase difference, Δ_{phase} which are not accounted for. The objective of this section is just to prove that EXAFS has the ability to measure local geometry of a given sample. In principle, multiple scattering occurs where there are more than 1 scattering atom. It may seem to pose as a

challenging issue but multiple scatterings are not a big problem as the amplitude of the backscatter waves from scattering atoms that are further are small and can be neglected.

EXPERIMENT AND DATA ANALYSIS

2.1 Introduction of Research

At the start of this project in Aug 2018, I was presented with a graph (Fig 2.1) given by my supervisor and I was asked to research on what the graph meant.

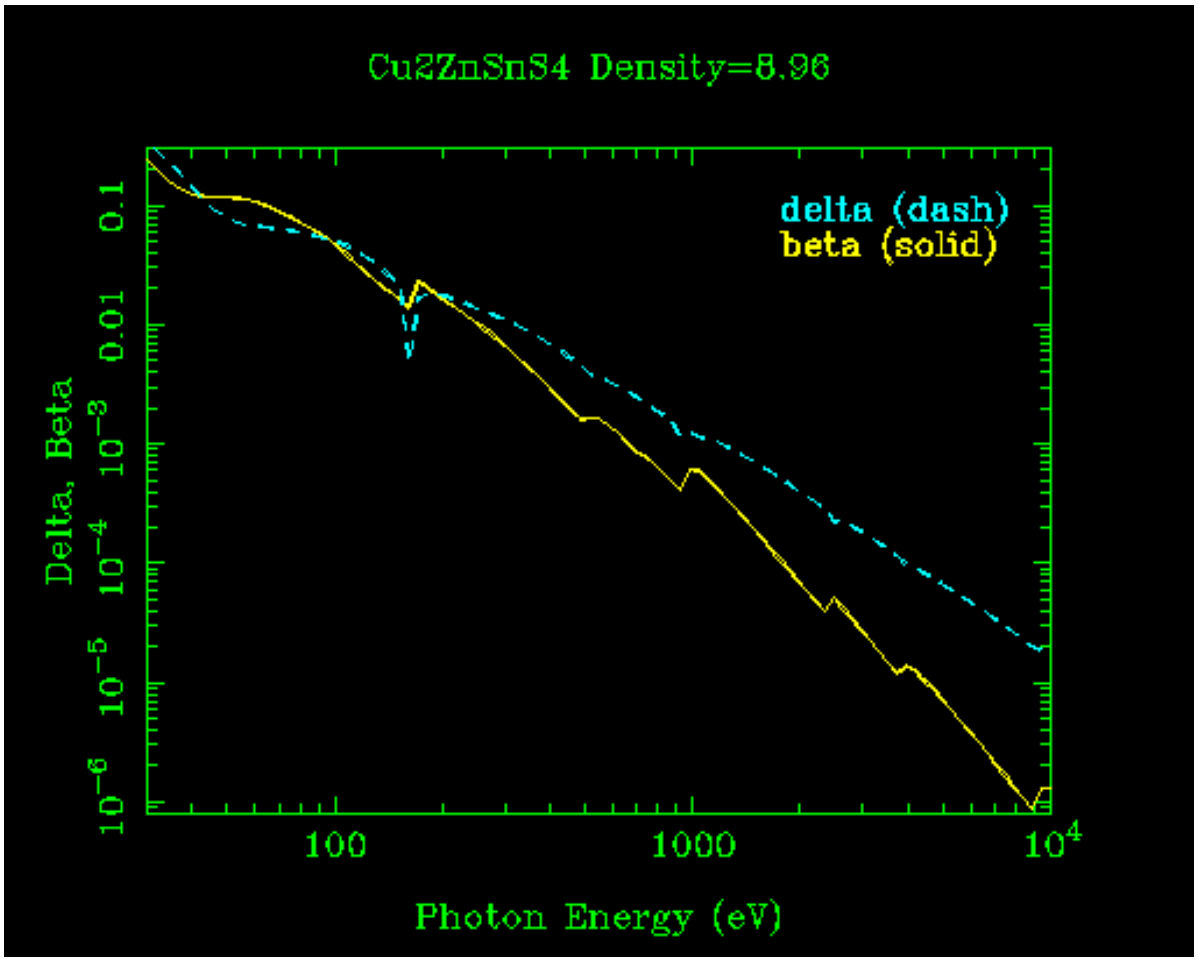

Figure 2.1 Graph of X-ray refractive index against incident photon energy.

Throughout the time I was researching on the technicalities of the graph, I was overwhelmed with even more questions which I seek to explain in the following sections. My project is based heavily on researching and the understanding of the theories and practicalities of the different categories of X-ray absorption spectroscopy. The source of the graph is from an online X-ray database provided by The Centre for X-ray Optics (CXRO), a multi-disciplined research group based in Lawrence Berkeley National Laboratory's (LBNL) Materials Sciences Division.

2.2 X-ray refractive index; Delta and Beta

As a start to uncover the graph that looked foreign to me, the first thing that I wanted to find out was what the axes meant.

(Fig. 2.1) shows the value of Delta and Beta on the y-axis and incident photon energy from the synchrotron light sourceon the x-axis. Just like visible light, X-rays have refractive index. Delta and beta are the terms of the refractive index of x-rays and the refractive index can be written in the form (Eq. 8)

$$n^* = 1 - \delta + i\beta \qquad (8)$$

where $1 - \delta$ = n in the conventional refractive index (Eq. 9)

$$n^* = n + i\beta \qquad (9)$$

The x-ray refractive index is similar to conventional refractive index; hence the refraction law of X-ray follows that of visible light which is described by the snell's law (Eq. 10)

$$\frac{n_1}{n_2} = \frac{\sin\theta_2}{\sin\theta_1} \qquad (10)$$

where n_1 and n_2 are two different mediums and θ_1 and θ_2 represents the angle of incident light or x-rays with respect to the normal of the plane.

X-ray refraction is described by (Eq. 8). where $1 - \delta$ represents the real part and β represents the imaginary part. Delta represents the refractive index decrement while Beta represents the absorption index.

Delta and beta are both related to f_1 and f_2, also called the atomic scattering factor.

2.3 Atomic Scattering factor

f_1 and f_2 are called the atomic scattering factor. They are related to delta and beta by the following equations (Eq. 11) and (Eq. 12)

$$\delta = \frac{n_a r_e \lambda^2}{2\pi} f_1 \qquad (11)$$

$$\beta = \frac{n_a r_e \lambda^2}{2\pi} f_2 \qquad (12)$$

where n_a is the number density, r_e is the classical electron radius and λ is the wavelength of the incident photon.

The atomic scattering factors measure how strongly an atom scatter the incident x-ray. Every different atom or element has very different scattering factor. This also means that different elements have different values of delta and beta. The difference between atomic scattering factor f_1 and f_2 is that f_1 describes the dispersive aspects of

scattering while f_2 describes the absorptive aspects of scattering.

Since the atomic scattering factor represents the absorptive and dispersive aspects of the scattering process, they can serve to describe how x-rays interact with samples or materials.

In XAS, f_2 for example will increase significantly at absorption edges. This is due to the increased absorption when incident photon energy corresponds to the binding energy of core electrons.

Other than the specific patterns at absorption edges, atomic scattering factors are affected by atomic number, Z. (Fig 2.2) and (Fig 2.3) shows how atomic scattering factor changes with atomic number, Z at different incident photon energies.

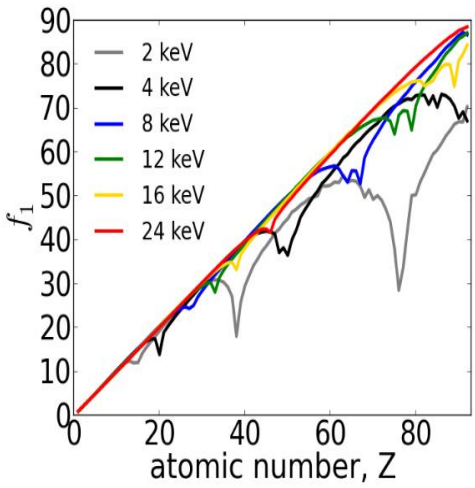

Figure 2.2 Atomic scattering factor f1 against atomic number, Z

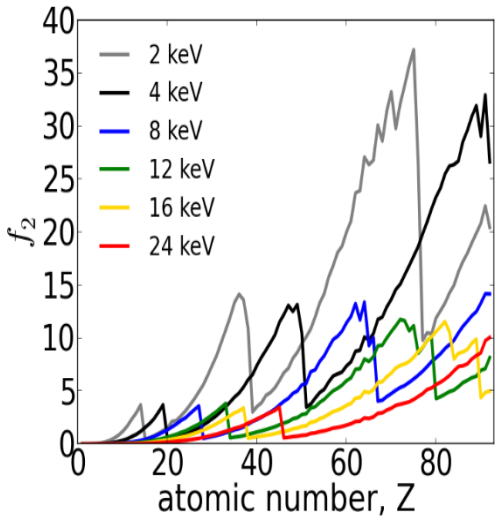

Figure 2.3 Atomic scattering factor f2 against atomic number, Z

From (Fig 2.2) and (Fig 2.3) we can see that f_1 and f_2 changes with atomic number, Z. Both (Fig 2.2) and (Fig 2.3) both shows that f_1 and f_2 generally increase with larger atomic number. This is due to the fact that X-ray interacts with electron cloud of the atom. A larger atomic number, Z means the larger the electron cloud and hence, the larger the scattering.

We can also clearly observe that at specific atomic number, there is a sharp decrease in f_1 in (Fig 2.2) and a sharp increase in f_2 in (Fig 2.3).

For example, let us look at 2keV (grey line), we observe that there is a sharp decrease or increase in f_1 and f_2 at atomic number ~ 40.

2.4 Atomic scattering factor database by CXRO

The online x-ray database of CXRO provides a database of atomic scattering factors of most of the elements in the periodic table (Fig 2.4).

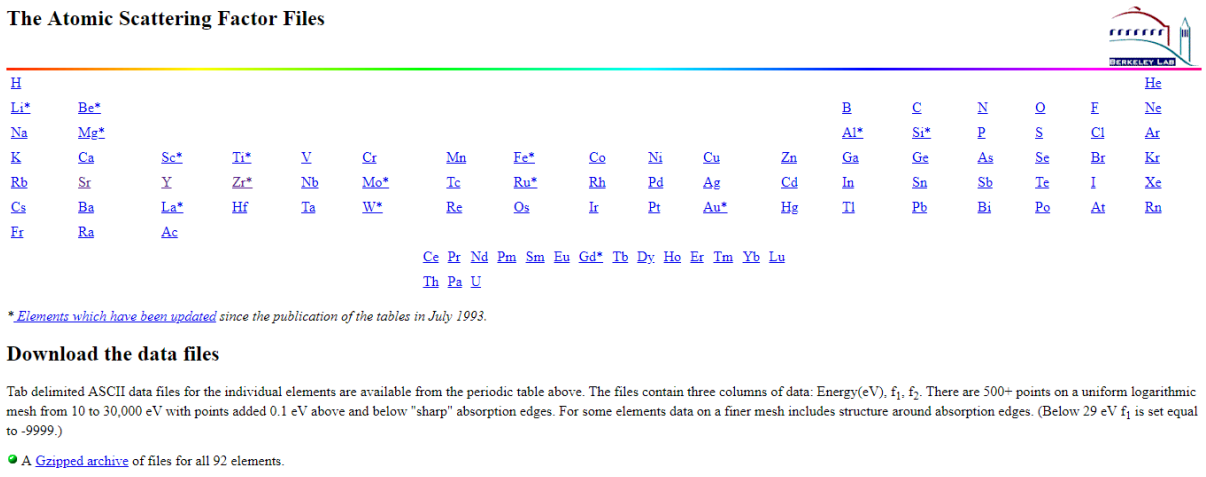

Figure 2.4 The atomic scattering factor files database provided by CXRO webpage.

To find out what is the element that contribute to the sharp decrease in f_1 and sharp increase in f_2 as observed in (Fig 2.2) and (Fig 2.3), I decided to download the data files of elements Z=40 (Zirconium), Z=39 (Yttrium) and Z=38 (Strontium).

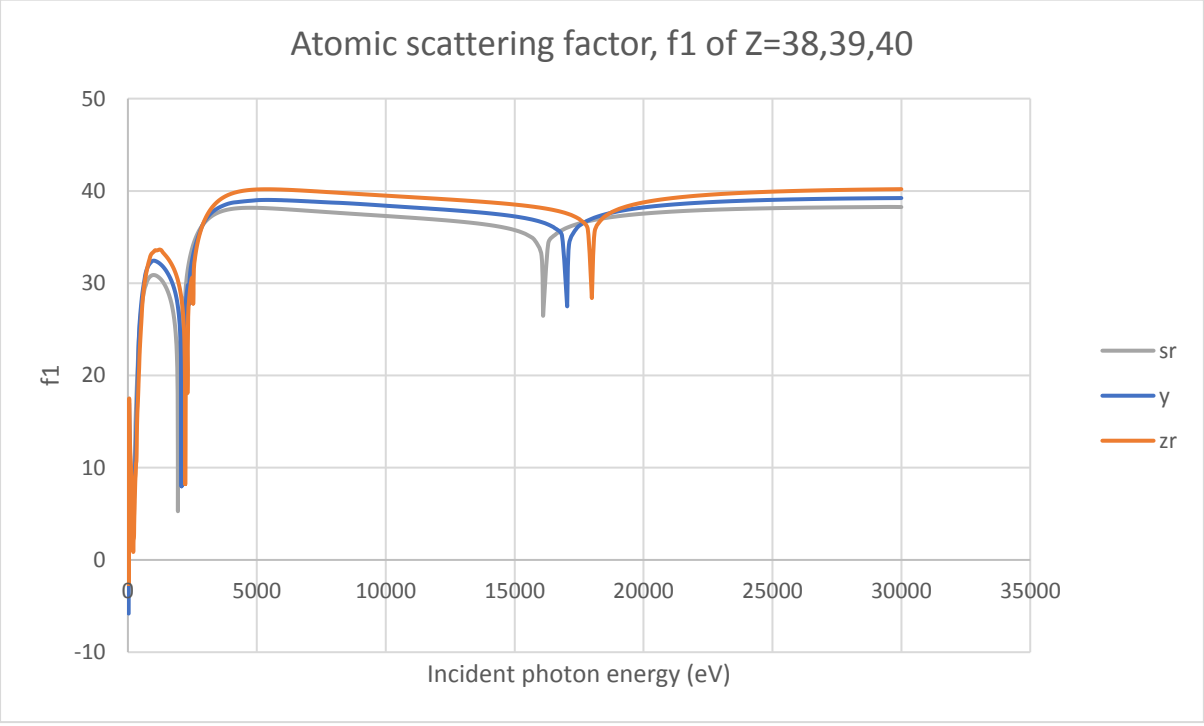

Figure 2.5 Graph of f1 against incident photon energy of Strontium -38, Yttrium -39, and Zirconium -40

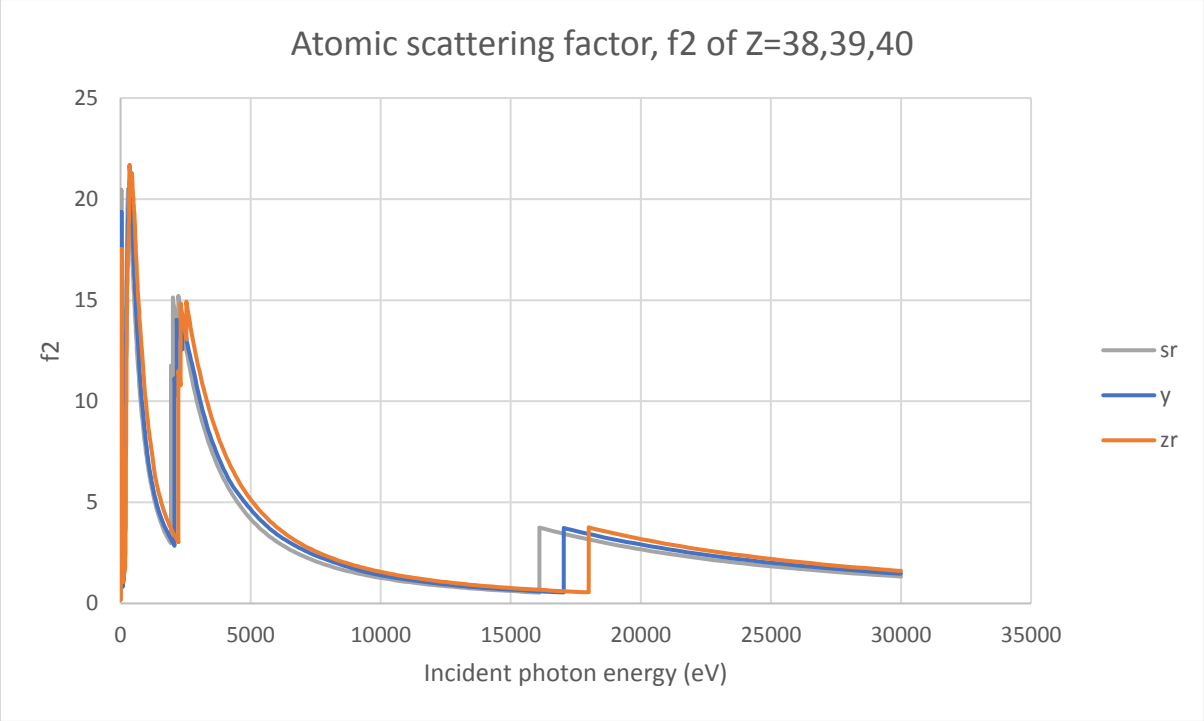

Figure 2.6 Graph of f2 against incident photon energy of Strontium -38, Yttrium -39, and Zirconium -40

The atomic scattering factor data files provided by CXRO has a range of 10eV to 30keV. After downloading the atomic scattering factor f_1 and f_2 of Strontium, Yttrium and Zirconium, the data were transferred into Microsoft Excel where the data were graphed using “Scatter with straight lines”. As seen on (Fig 2.5) and (Fig 2.6), both atomic scattering factors have sharp edges at ~2keV. This shows that indeed the dispersive edges and absorption edges in (Fig 2.2) and (Fig 2.3) are justifiable.

One obvious observation that can be seen from (Fig 2.5) and (Fig 2.6) is that the value of f_1 and f_2 are generally higher with higher Z, as mentioned earlier. Also, the edges occur at lower incident photon energy for lower Z (the edges of the grey Strontium line are always on the left of Yttrium and Zirconium). To observe the edges at ~2keV, the graph are replotted to limit incident photon energy from 1keV to 3keV and are presented in the following page (Fig 2.7) and (Fig 2.8).

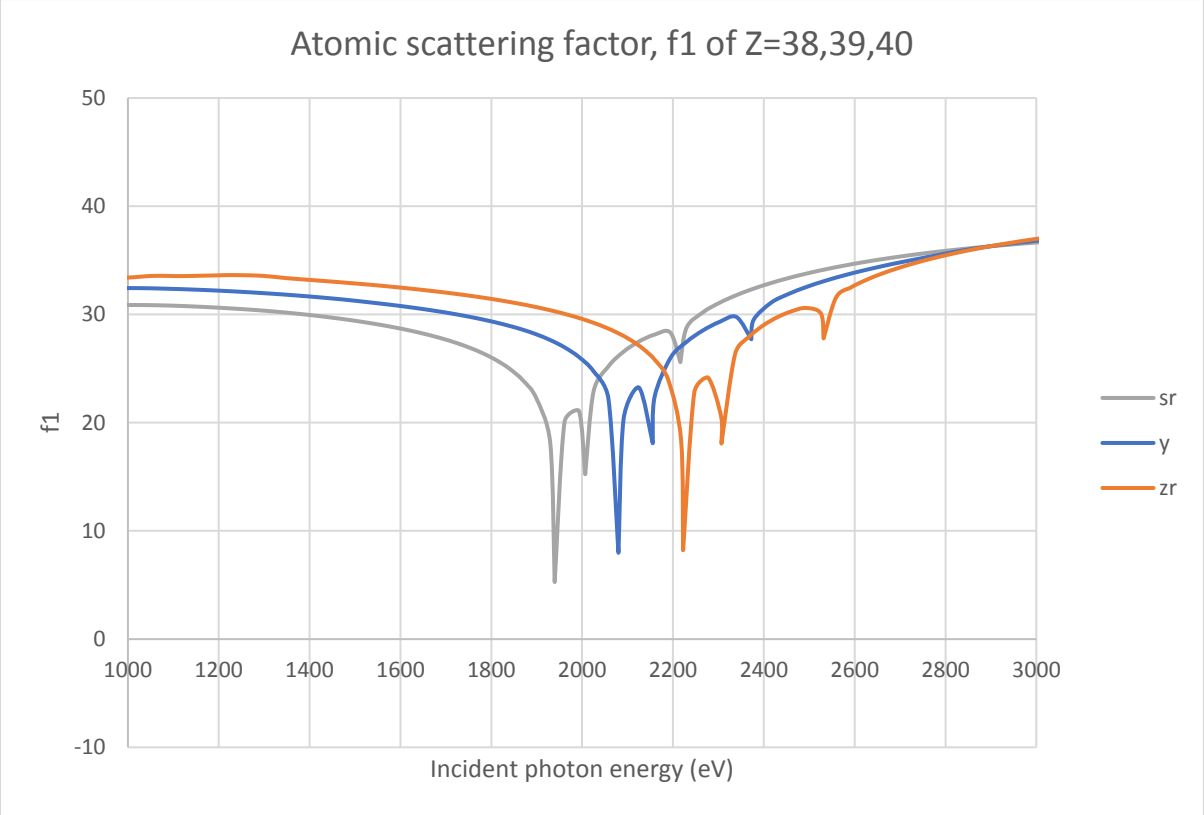

Figure 2.7 Graph of f1 against incident photon energy of Strontium -38, Yttrium -39, and Zirconium -40 (1keV to 3keV)

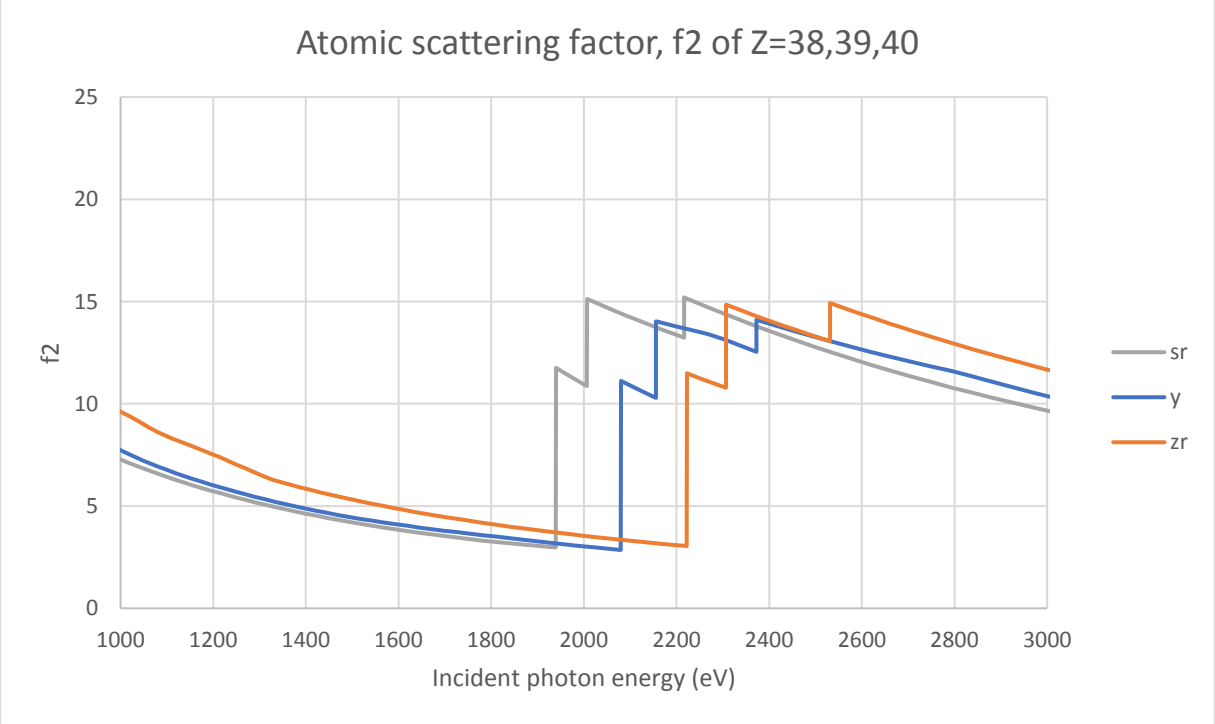

Figure 2.8 Graph of f2 against incident photon energy of Strontium -38, Yttrium -39, and Zirconium -40 (1keV to 3keV)

When the data of incident photon energy is zoomed into the 1keV to 3keV region, we observed that the seemingly singular edge actually has several edges.

Let us look at Strontium in particular as the edges are closest to 2keV. Strontium is an alkali earth metal with Z=38. Strontium has edge energies of the following (Fig 2.9)

Edge Energies (keV)	
K	16.1049995
L1	2.21600008
L2	2.00699997
L3	1.94000006
M	0.35800001
K-alpha	14.1639996
K-beta	15.8339996
L-alpha	1.80599999
L-beta	1.87199998

Figure 2.9 Edge energies of Strontium.
Photo from www.yourperiodictable.com/strontium

(Fig 2.9) shows the edge energies of Strontium; the K-edge, L1, L2 and L3 edges are all shown on the table. Comparing the values of the absorption edges of (Fig 2.7), we realised that the three edges of Strontium at ~2keV belong to the L3, L2 and L1-edges from left to right.

This shows that the data provided by CXRO are able to identify precisely the value of the different edges.

2.5 CXRO's calculation of atomic scattering factor f_1 and f_2

(Eq. 11) and (Eq. 12) both represent how delta and beta is related to f_1 and f_2 but does not present how the value of f_1 and f_2 is derived.

f_2, the absorption aspect of the atomic scattering factor, is calculated from photoabsorption crosssection σ_a, shown in (Eq. 13)

$$f_2 = \frac{\sigma_a}{2r_e\lambda} \qquad (13)$$

Photoabsorption crosssection, σ_a describes the probability of an absorption process. The CXRO database of atomic scattering factor are calculated using (Eq. 13) by means of measuring photoabsorption crosssection σ_a of elements in their elemental state experimentally. CXRO states that the atomic scattering factor for condensed matter such as Cu_2ZnSnS_4 "*may be modelled as a collection of non-interacting atom. This assumption is in general a good one for energies sufficiently far from absorption edges.*"

2.6 Attempt to understand CXRO's method of calculation by trying to recreate (Fig 2.1)

Let us analyse the CXRO's method of calculating scattering factor of condensed matter.

First of all, I believe that the refractive index terms of Cu_2ZnSnS_4 (Fig 2.1), delta and beta are derived from (Eq. 11) and (Eq. 12) which relates delta with f_1 and beta with f_2.

Hence the following are my steps to find out how the graph shown on (Fig 2.1) is calculated.

1. Since it was mentioned in CXRO's webpage that the scattering factor of condensed matter can be treated as non-interacting atoms, I would like to sum up the atomic scattering factor of all the individual stoichiometry components in Cu_2ZnSnS_4.

2. After obtaining the proposed scattering factor of Cu_2ZnSnS_4, I wish to translate it into its delta and beta.

3. Find out how CXRO converts its scattering factor into delta and beta.

4. Apply this method of conversion to the scattering factor that is calculated in step 2.

5. Reproduce the graph shown in (Fig 2.1) to check whether my methods are analogous to CXRO's methods.

The CXRO online database do not have a platform for direct calculation of scattering factor of condensed matter such as Cu_2ZnSnS_4, hence the need for step 1.

Also, I believe that the refractive index terms delta and beta, are calculated based on the atomic scattering factor with the relation of (Eq. 11) and (Eq. 12). Hence, I would try to find out if delta and beta are related to both f1 and f2 with a constant term. If they are related to a constant term, we can input this constant term into the scattering factor of the condensed matter as calculated in step 1 and reproduce the graph.

RESULTS AND DISCUSSIONS

3.1 Summing of Atomic Scattering factors

The individual atomic scattering factors are provided by CXRO's online database. The graph of atomic scattering factor f_1 and f_2 are presented in the APPENDIX (Fig S1 – S6) These graphs are plotted with incident photon energy ranging from 0eV to 30keV.

Since the graph handed to me by my supervisor (Fig 2.1) has its incident photon energy ranging from 10eV to 10keV, the atomic scattering factor data that we obtained from the database of CXRO's webpage are chosen from 10eV to 10keV.

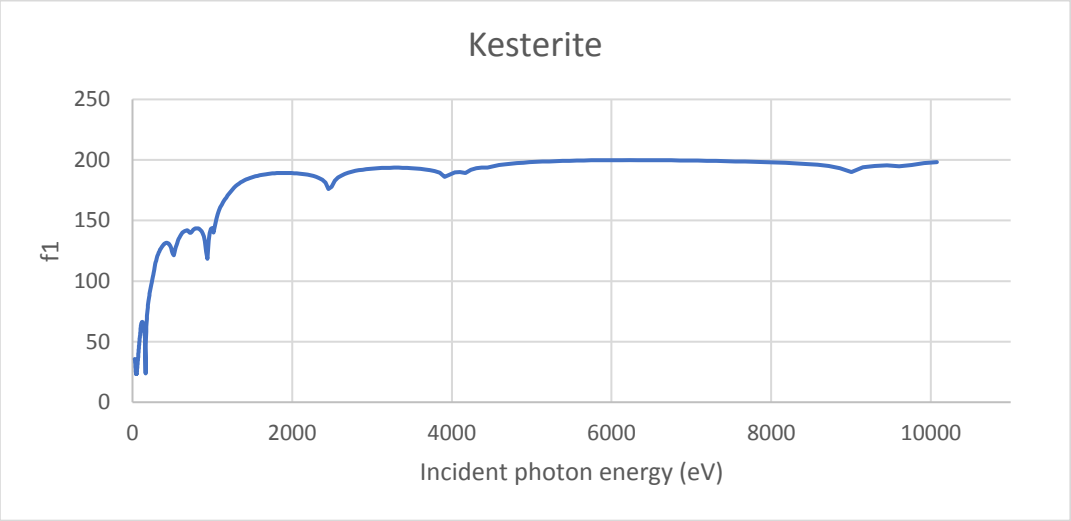

Figure 3.1 Scattering factor f1 of Cu2ZnSnS4, Kesterite.

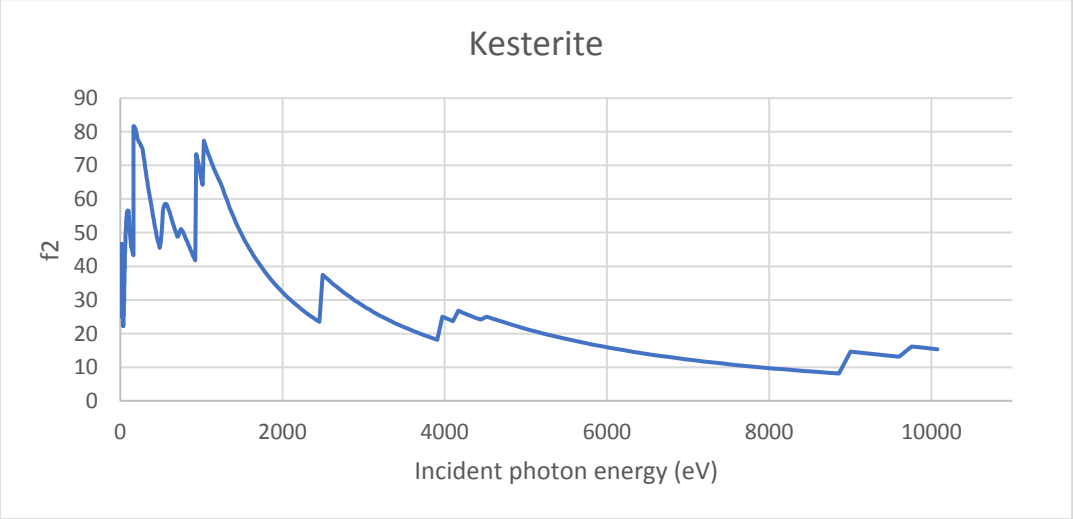

Figure 3.2 Scattering factor f1 of Cu2ZnSnS4, Kesterite.

(Fig 3.1) and (Fig 3.2) shows the scattering factor of Cu_2ZnSnS_4, Kesterite. It is obtained by summing up the individual elements Cu, Zn, Sn and S. It is done by a simple summation given by (Eq 14)

$$Scattering\ factor\ of\ kesterite = Atomic\ scattering\ factor\ of\ 2CU + Zn + Sn + 4S \quad (14)$$

The basis of this calculation is due to the model described by CXRO as 'non-interacting atoms'.

3.2 Relationship between delta and f1 and between beta and f2

In the CXRO's webpage, there exists a tool called "Look up X-ray properties of the elements" which is shown in (Fig 3.3)

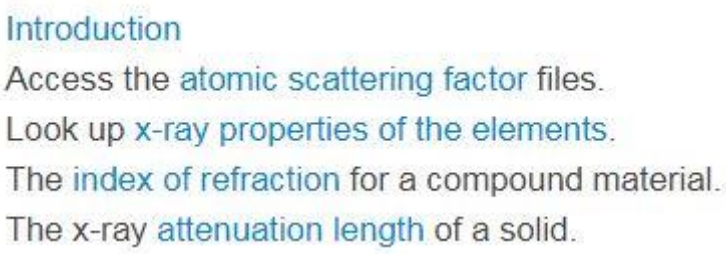

Figure 3.3 CXRO webpage showing the different tools

Element symbols are submitted with their corresponding incident photon energy and a list of x-ray properties of the element will be given. These properties include atomic scattering factor f_1 and f_2 and refractive index delta and beta. My postulation was that f_1 and f_2 are related to delta and beta respectively by (Eq. 11) and (Eq. 12) by a constant

$$\delta = \frac{n_a r_e \lambda^2}{2\pi} f_1 \quad (11)$$

$$\beta = \frac{n_a r_e \lambda^2}{2\pi} f_2 \quad (12)$$

where the constant is the term $\frac{n_a r_e \lambda^2}{2\pi}$ present in both (Eq 11) and (Eq 12).

For a start, the x-ray properties of copper at 1000eV were obtained with the CXRO tool. The following properties are given by the webpage

$f_1 = 16.61$

$f_2 = 16.20$

Delta = 9.7222×10^{-4}

Beta = 9.4858×10^{-4}

Using these values, the value of the constant term $\frac{n_a r_e \lambda^2}{2\pi}$ can be determined from (Eq. 15) and (Eq. 16)

From f1 and delta:

$$\frac{n_a r_e \lambda^2}{2\pi} = \frac{\delta}{f_1} \qquad (15)$$

$$= 5.5832 \times 10^{-5}$$

From f2 and beta:

$$\frac{n_a r_e \lambda^2}{2\pi} = \frac{\beta}{f_2} \qquad (16)$$

$$= 5.5855 \times 10^{-5}$$

The percentage difference between the two constant terms are 0.00411%; a small percentage difference means that indeed f_1 and f_2 are related to delta and beta by the same constant.

However, this only shows that the constant term is equal for (Eq. 11) and (Eq. 12) for copper at 1000eV. To check whether it is constant at other incident photon energy levels, 20 other incident photon energy values for copper are plugged into the CXRO tool ranging from 30eV to 10000eV. These 20 data are plugged into (Table S1)

The results showed that at all energy range from 30eV to 10000eV, the constant term that is calculated by (Eq. 15) and (Eq. 16) has very small percentage difference. This concludes that for the same material at the same incident photon energy, the constant term $\frac{n_a r_e \lambda^2}{2\pi}$ is the same for (Eq 11) and (Eq 12)

However, the results also showed that at higher energy levels, the value of the constant term $\frac{n_a r_e \lambda^2}{2\pi}$ decreases as incident photon energy increases. The reason is obvious; at higher energy level, wavelength of x-ray decreases while the other terms stay constant.

We recall that:

r_e is the classical electron radius = 2.8179 x 10^{-15},

$\lambda = \frac{hc}{E}$ where λ is the wavelength of the incident x-ray, E is the incident photon energy,

and n_a is the number density which can be expressed as

$$n_a = \frac{\rho N_a}{M_a} \qquad (17)$$

where ρ is the physical density of the material, N_a is the Avogadro's constant and M_a is the molar mass of the material. The theoretical value of n_a of copper was calculated to be 8.487 x 10^{28}. The value of n_a calculated by using the values of f1 and f2 given by CXRO has very small percentage discrepancy as seen in (Table S1).

This section shows that the refractive index delta and beta can be confidently determined using scattering factor f_1 and f_2 as long as we know the physical density of the material and the molar mass of the material.

3.3 Translating the scattering factor of Kesterite into delta and beta

As mentioned in the previous section, to determine delta and beta from (Fig 3.1) and (Fig 3.2), we require the constant term, $\frac{n_a r_e \lambda^2}{2\pi}$ where the only variables are n_a and λ^2. Hence, by finding the number density n_a of Kesterite, it is possible to translate the scattering factor into delta and beta and the graph (Fig 2.1) can be recreated and compared.

According to (Eq 17), the number density of Kesterite can be derived. The molar mass, M_a of Kesterite is 439.471g/mol. Its physical density, ρ is 4.56g/cm^3. The number density of Kesterite is calculated to be n_a = 6.246 x 10^{27} / m^3. We plug this value back to (Eq. 11) and (Eq. 12) to find out the values of delta and beta for

Kesterite. The values obtained are used to plot a graph of delta against incident photon energy and a graph of beta against incident photon energy.

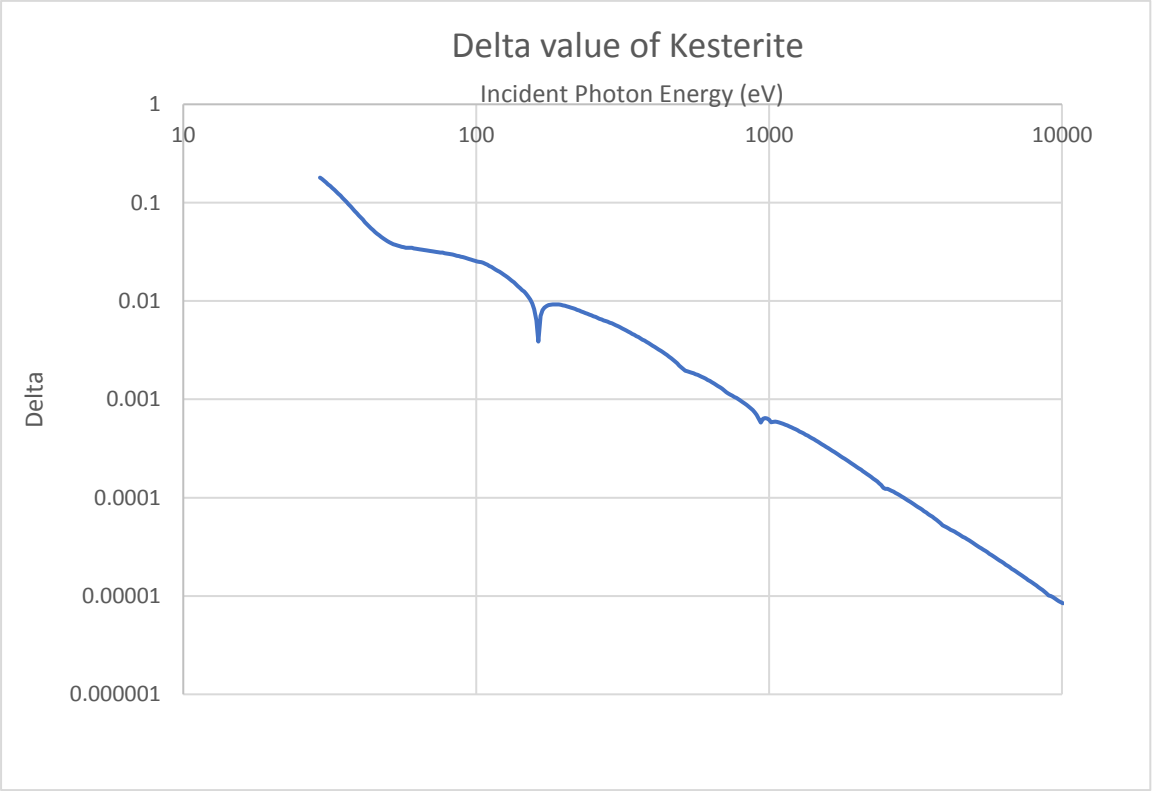

Figure 3.4 Delta value of Kesterite using individual atomic scattering factors - Model of non-interacting atoms

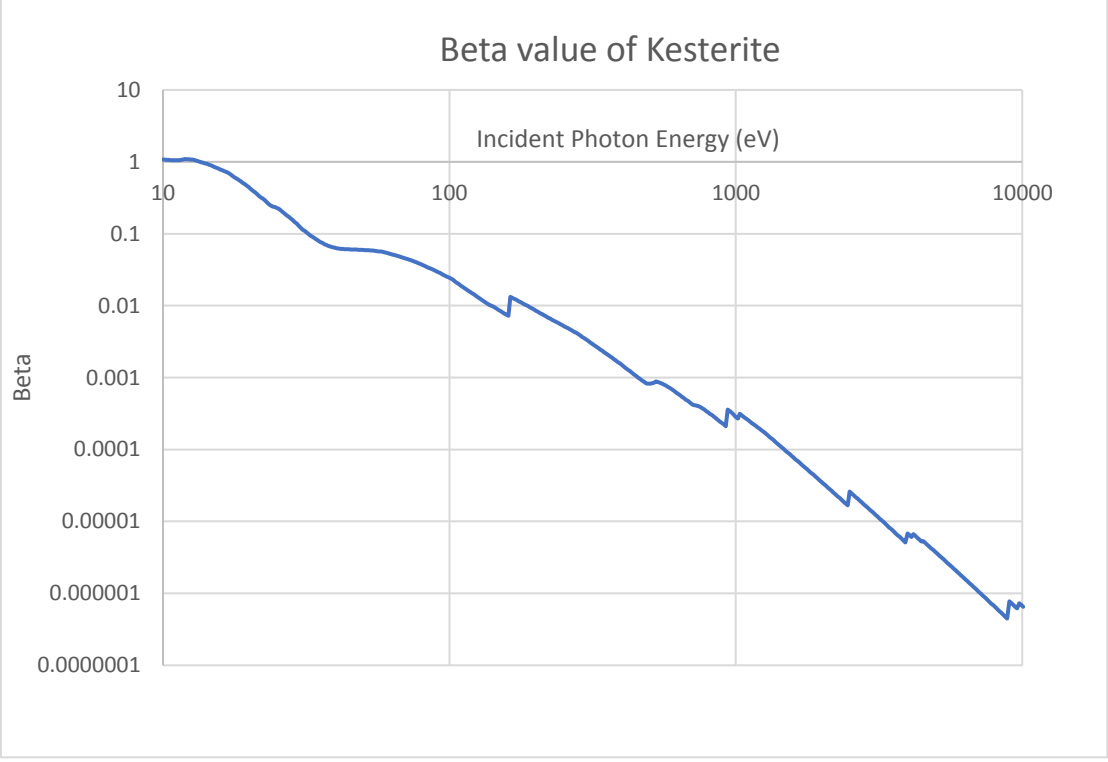

Figure 3.5 Belta value of Kesterite using individual atomic scattering factors - Model of non-interacting atoms

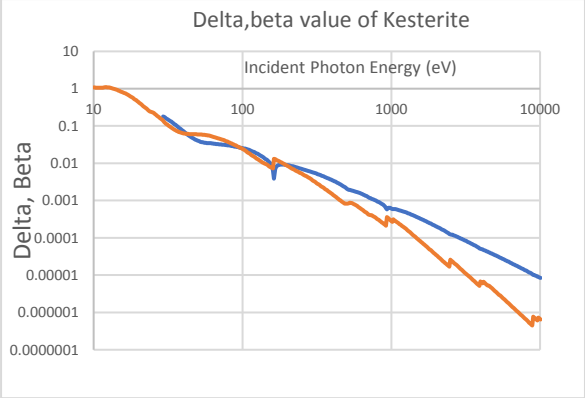

Figure 3.6 Combining (Fig 3.4) and (Fig 3.5) on the same graph

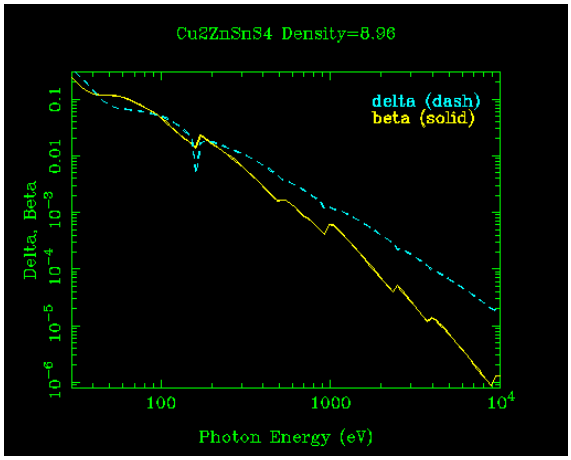

Figure 3.7 Graph that was initially presented to me by my supervisor (Fig 2.1)

Comparing (Fig 3.6) and (Fig 3.7), it shows that indeed, scattering factor of condensed matter such as that of Cu_2ZnSnS_4, Kesterite can be well modeled as a group of non-interacting atoms to a certain extent.

3.4 Comparing the graphs in details

In general, the shapes of the two graphs are similar. It is to note once again that (Fig 3.6) was calculated by summing up the individual atomic scattering factors and then converted to the values delta and beta by introducing the constant term $\frac{n_a r_e \lambda^2}{2\pi}$. On the other hand (Fig 3.7 / Fig 2.1) is obtained by plugging in the formula Cu_2ZnSnS_4 directly into the online CXRO tool.

However, to compare the two graphs in details, the calculated beta value is plotted on the same graph as the beta value that CXRO provided.

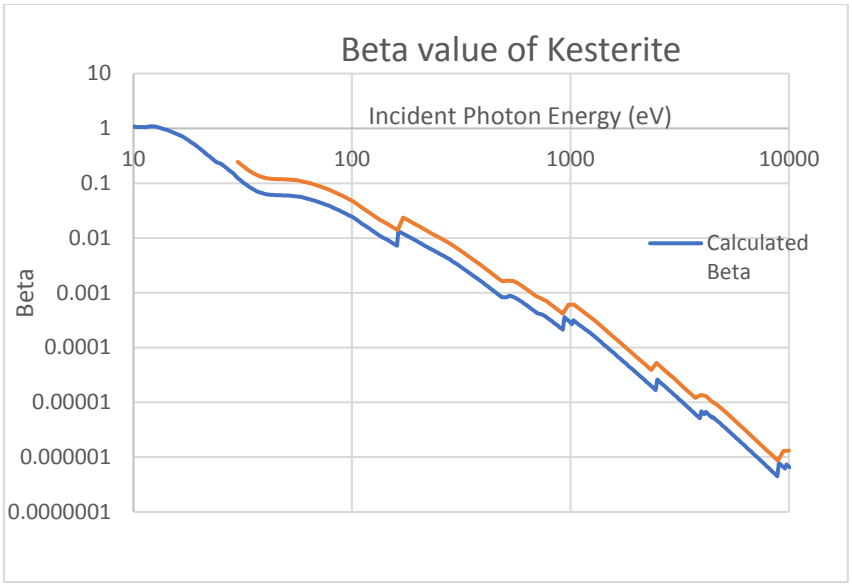

Figure 3.8 Comparing beta values of Kesterite.

The reason for the difference in the value lies in the density of Kesterite plugged into the CXRO calculator. The density, ρ of Kesterite is 4.56g/cm^3. The CXRO webpage explained that "*if a negative density value is entered, the chemical formula is checked against a list of some common materials. If no match is found then the density of the first element in the formula is used*" which in this case is Copper with a density, ρ of 8.96g/cm^3. When the correct density of Kesterite is plugged into the CXRO calculator, we compare the two beta values again to see that it fits almost perfectly to our calculated values.

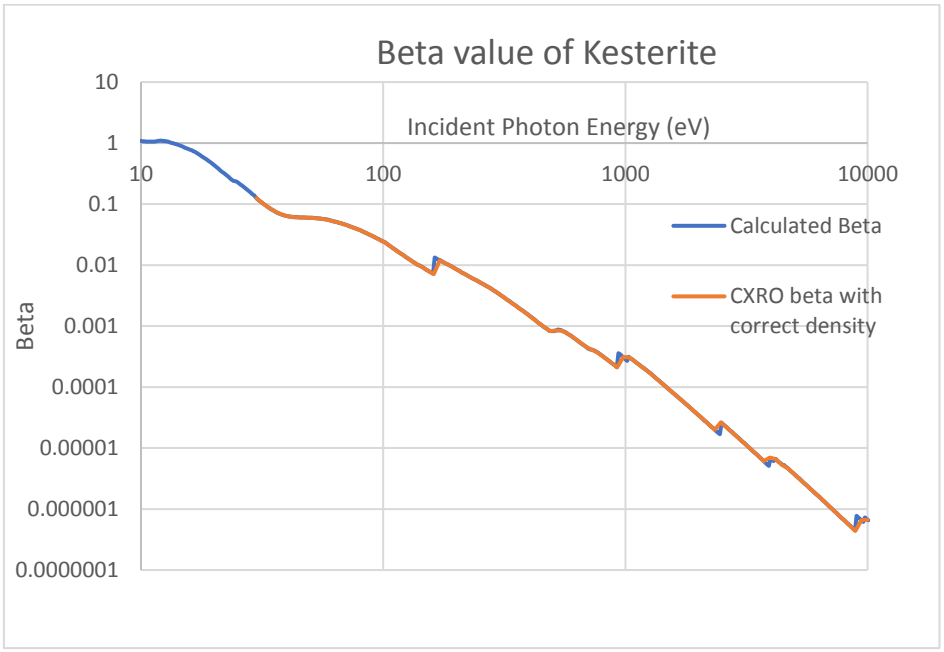

Figure 3.9 Comparing beta values of Kesterite with corrected density of Cu2ZnSnS4

CONCLUSION AND FUTURE WORK

The aim of this project was to understand the technicalities of XAS. XAS has shown to be a useful method in deducing the elemental composition of unknown materials. As compared to other methods such as XES, XAS is unique for its ability to investigate the local geometric of samples in the EXAFS region; to calculate interatomic distance of crystals. XANES such as Metal K-edge and Metal L-edge spectroscopy not only shows the element present in the sample but also the electron spin e.g. in L1, L2 and L3 edges. This allows for us to understand the electronic configuration of the elements present in the sample. The many useful applications of XAS convinced me that cost of building synchrotron radiation facilities are justifiable.

Also, the model of calculating scattering factor of condensed matter such as Kesterite by assuming that the compound is a group of non-interacting atoms was shown to be a rather good approximation. Using this idea, the scattering factor of many unknown compounds can be calculated by breaking down the compound into their elements. Hence, by knowing the physical density of the material, we are able to model with good approximation the x-ray refractive index of the material, which is a fundamental physical property of a material.

REFERENCES

1. Ascone, I. (2011). *X-ray absorption spectroscopy for beginners*. [online] Iucr.org. Available at: https://www.iucr.org/__data/assets/pdf_file/0004/60637/IUCr2011-XAFS-Tutorial_-Ascone.pdf
2. Ravel, B. (2015). *Introduction to X-ray Absorption Spectroscopy*. [online] Bnl.gov. Available at: https://www.bnl.gov/ps/userguide/lectures/Lecture-4-Ravel.pdf
3. Gisaxs.com. *Refractive index - GISAXS*. [online] Available at: http://gisaxs.com/index.php/Refractive_index
4. Gullikson, E. (n.d.). *Atomic scattering factors*. [online] Xdb.lbl.gov. Available at: http://xdb.lbl.gov/Section1/Sec_1-7.pdf
5. Xdb.lbl.gov. (n.d.). *X-ray Data Booklet.* [online] Available at: http://xdb.lbl.gov/Section5/Sec_5-5.pdf
6. Gisaxs.com. (n.d.). *Atomic scattering factors - GISAXS*. [online] Available at: http://gisaxs.com/index.php/Atomic_scattering_factors
7. Henke.lbl.gov. (n.d.). *CXRO X-Ray Interactions With Matter*. [online] Available at: http://henke.lbl.gov/optical_constants/
8. B.L. Henke, E.M. Gullikson, and J.C. Davis. *X-ray interactions: photoabsorption, scattering, transmission, and reflection at E=50-30000 eV, Z=1-92*, Atomic Data and Nuclear Data Tables Vol. **54** (no.2), 181-342 (July 1993).
9. Brown, R. (2007). *Kramers-Kronig Relations*. [online] Webhome.phy.duke.edu. Available at: https://webhome.phy.duke.edu/~rgb/Class/phy319/phy319/node56.html
10. Penner-Hahn, J. (n.d.). *X-ray Absorption Spectroscopy*. [ebook] The University of Michigan, Ann Arbor, MI, USA, pp.159-182. Available at: https://www.elsevier.com/__data/promis_misc/622954sc1.pdf
11. X-ray Absorption Fine Structure (EXAFS). (n.d.). [ebook] p.Chapter 1. Available at: http://smb.slac.stanford.edu/~ellis/Thesis/Chapter1.pdf
12. Lytle, F. (1999). *The EXAFS family tree: a personal history of the development of extended X-ray absorption ®ne structure*. [ebook] The EXAFS Company, Pioche: J. Synchrotron Rad, pp.123-133. Available at: http://www.unm.edu/~ejpete/pdf/The%20EXAFS%20family%20tree%20a%20personal%20history%20of%20the%20development.pdf
13. MLA style: Charles Glover Barkla – Biographical. NobelPrize.org. Nobel Media AB 2019. Thu. 4 Apr 2019. https://www.nobelprize.org/prizes/physics/1917/barkla/biographical/

14. MLA style: The Nobel Prize in Physics 1915. NobelPrize.org. Nobel Media AB 2019. Thu. 4 Apr 2019. https://www.nobelprize.org/prizes/physics/1915/summary/
15. Albasynchrotron.es. (n.d.). *X-RAY EMISSION SPECTROSCOPY AVAILABLE — en*. [online] Available at: https://www.albasynchrotron.es/en/media/news/x-ray-emission-spectroscopy-available
16. Bergmann, Uwe & Glatzel, Pieter. (2009). X-ray emission spectroscopy. Photosynthesis research.
17. Bazylewski, P. (2011). *X-ray Spectroscopy*. [online] Physics.usask.ca. Available at: http://physics.usask.ca/~chang/homepage/xray/xray.html
18. Chemistry LibreTexts. (2016). *EXAFS: Theory*. [online] Available at: https://chem.libretexts.org/Bookshelves/Physical_and_Theoretical_Chemistry_Textbook_Maps/Supplemental_Modules_(Physical_and_Theoretical_Chemistry)/Spectroscopy/X-ray_Spectroscopy/EXAFS%3A_Theory
19. Sladecek, M. (2005). *The refractive index and Snell's law*. [online] Sladecek.org. Available at: http://www.sladecek.org/NRS/node12.html#Snell
20. J.H. Hubbell, W.J. Veigele, E.A. Briggs, R.T. Brown, D.T. Cromer, and R.J. Howerton, Atomic Form Factors, Incoherent Scattering Functions, and Photon Scattering Cross Sections, J. Phys. Chem. Ref. Data **4**, 471-538 (1975); erratum in 6, 615-616 (1977)
21. En.wikipedia.org. (n.d.). *Extended X-ray absorption fine structure*. [online] Available at: https://en.wikipedia.org/wiki/Extended_X-ray_absorption_fine_structure
22. En.wikipedia.org. (n.d.). *Refractive index*. [online] Available at: https://en.wikipedia.org/wiki/Refractive_index
23. Ida, T. (2013). *Crystal Structure Analysis*. [ebook] Graduate School of Engineering, Nagoya Institute of Technology, p.Chapter 2. Available at: http://www.crl.nitech.ac.jp/~ida/education/CrystalStructureAnalysis/2/2e.pdf
24. Ruppweb.org. (n.d.). *Scattering Factor Calculation*. [online] Available at: https://www.ruppweb.org/Xray/comp/scatfac.htm

APPENDIX

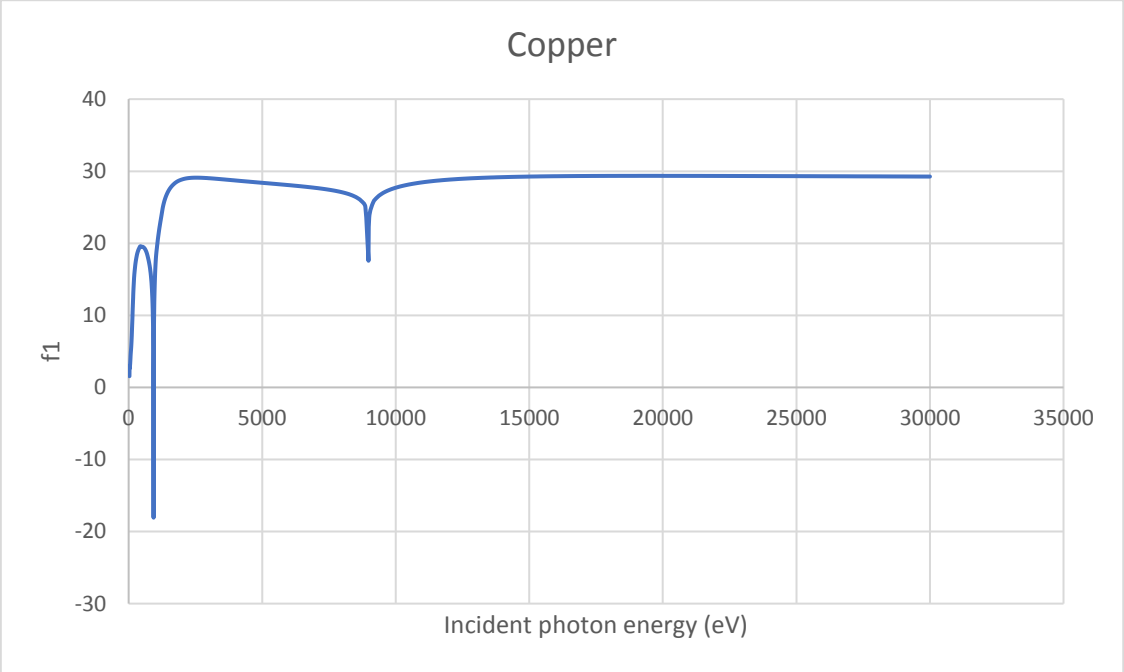

Figure S1 Atomic scattering factor f1 of Copper

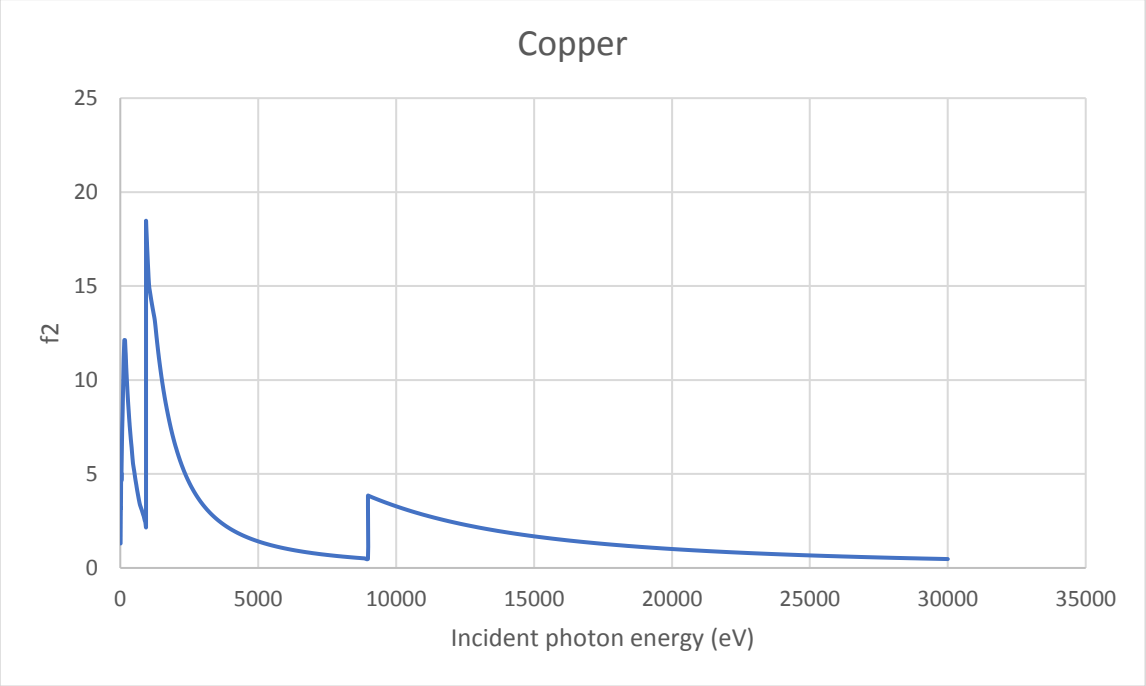

Figure S2 Atomic scattering factor f2 of Copper

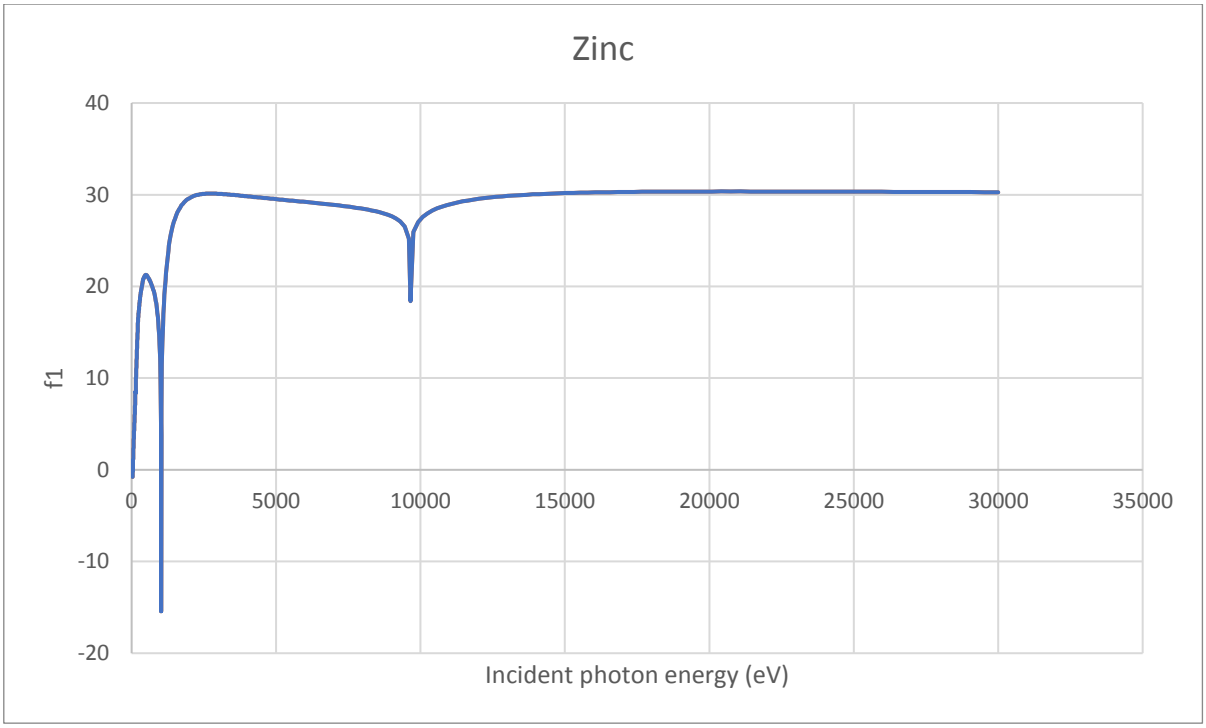

Figure S3 Atomic scattering factor f1 of Zinc

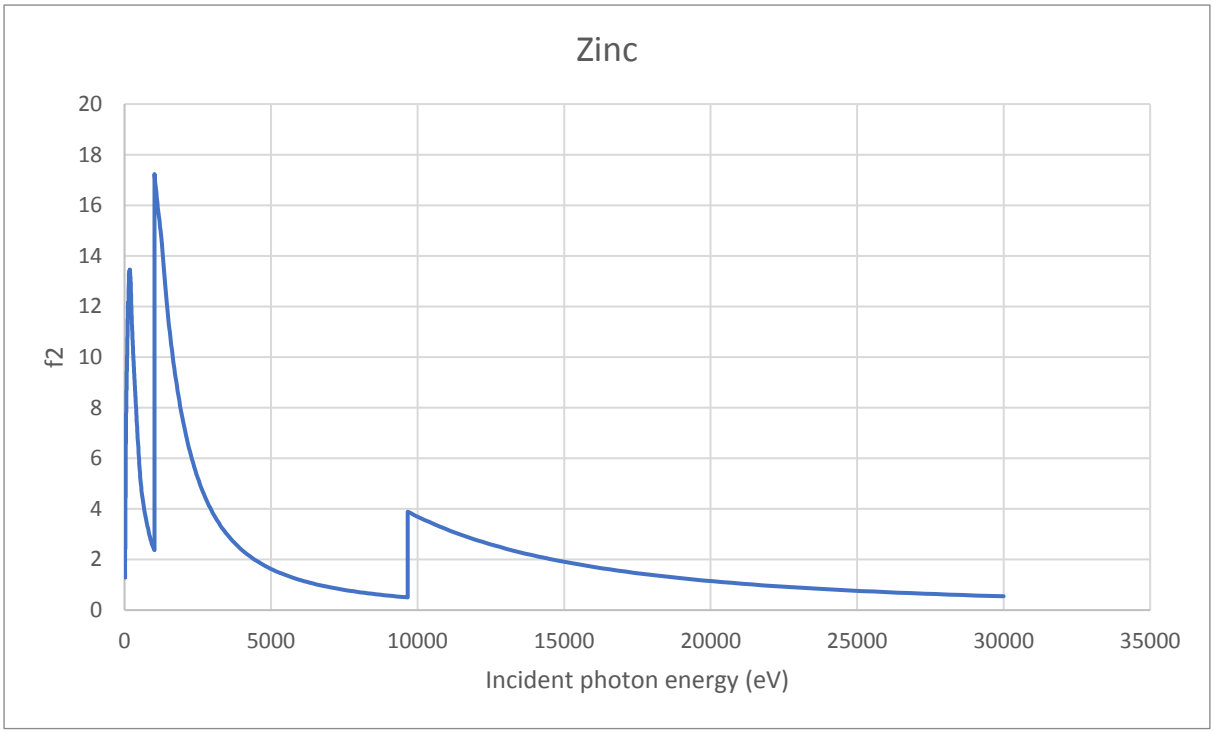

Figure S4 Atomic scattering factor f2 of Zinc

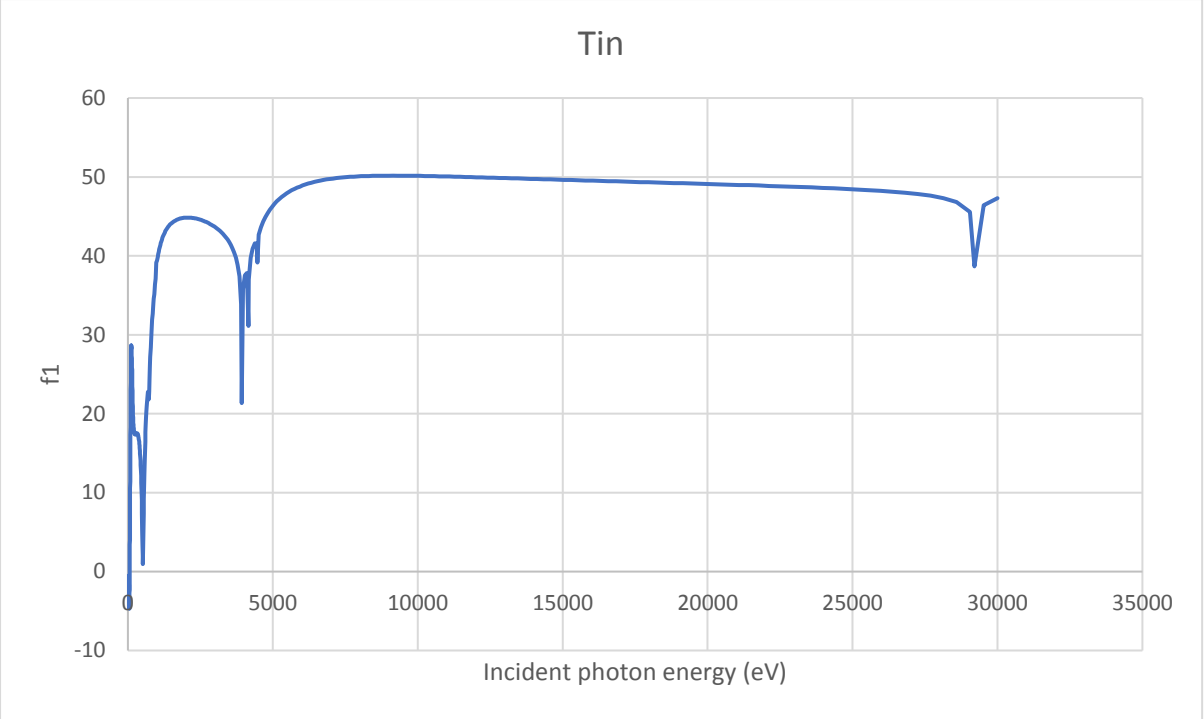

Figure S5 Atomic scattering factor f1 of Tin

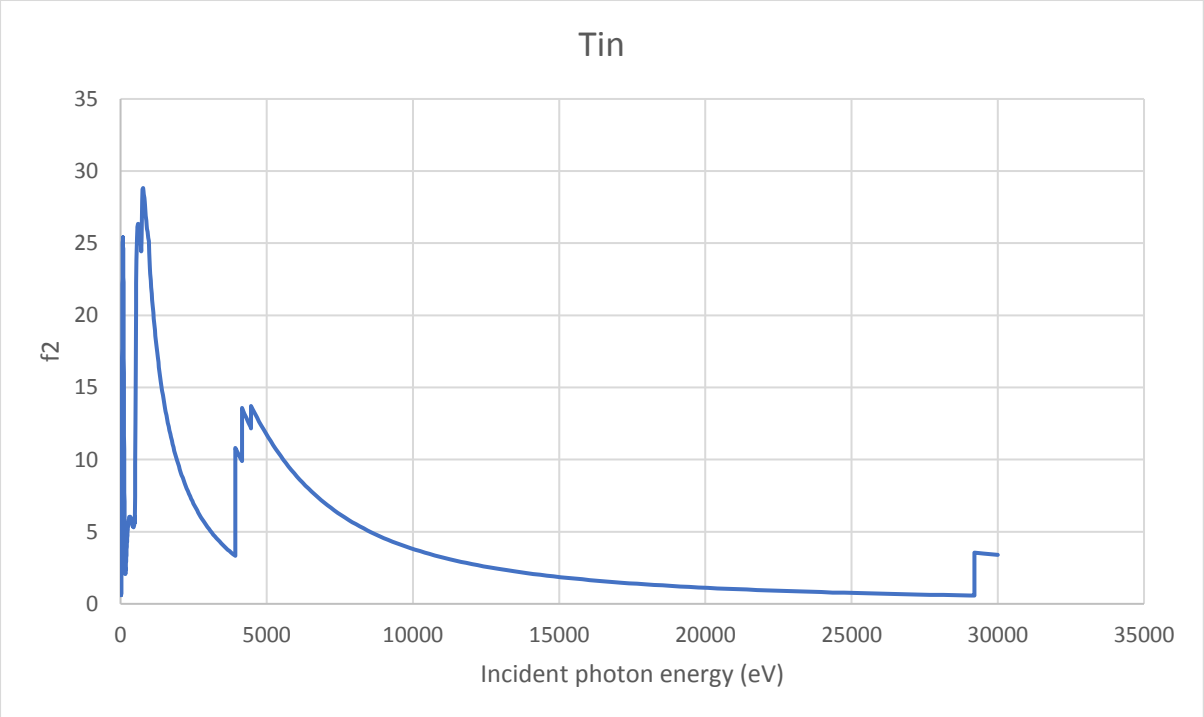

Figure S6 Atomic scattering factor f2 of Tin

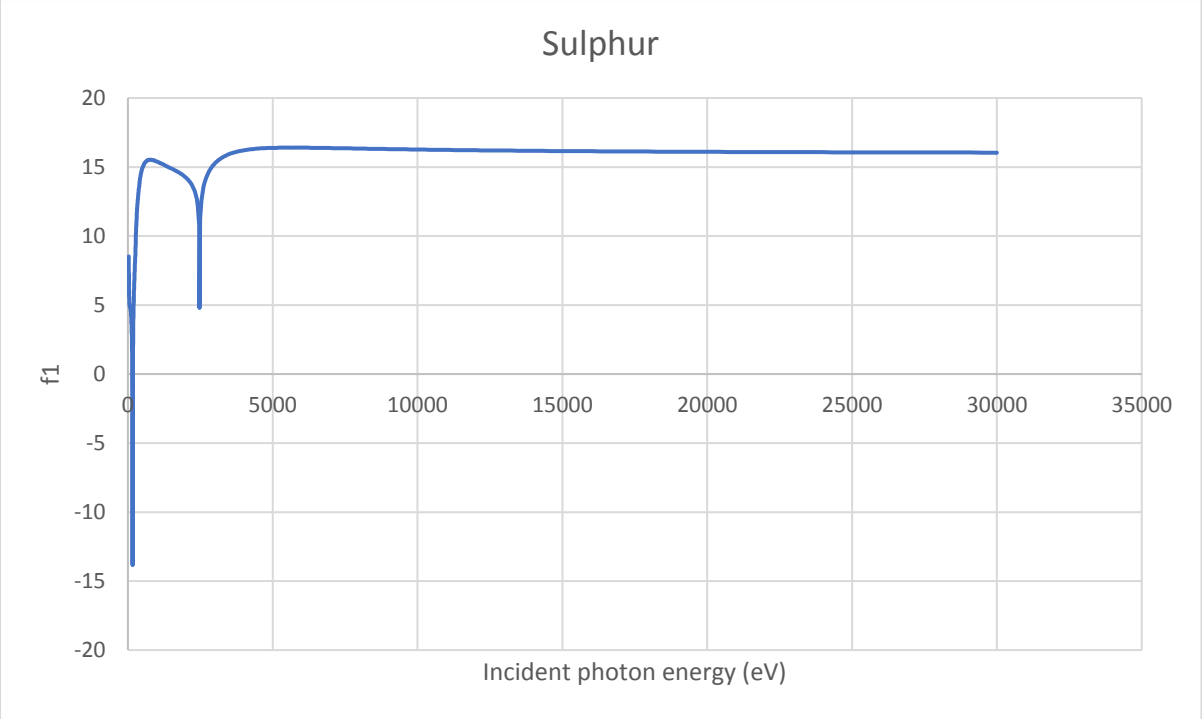

Figure S7 Atomic scattering factor f1 of Sulphur

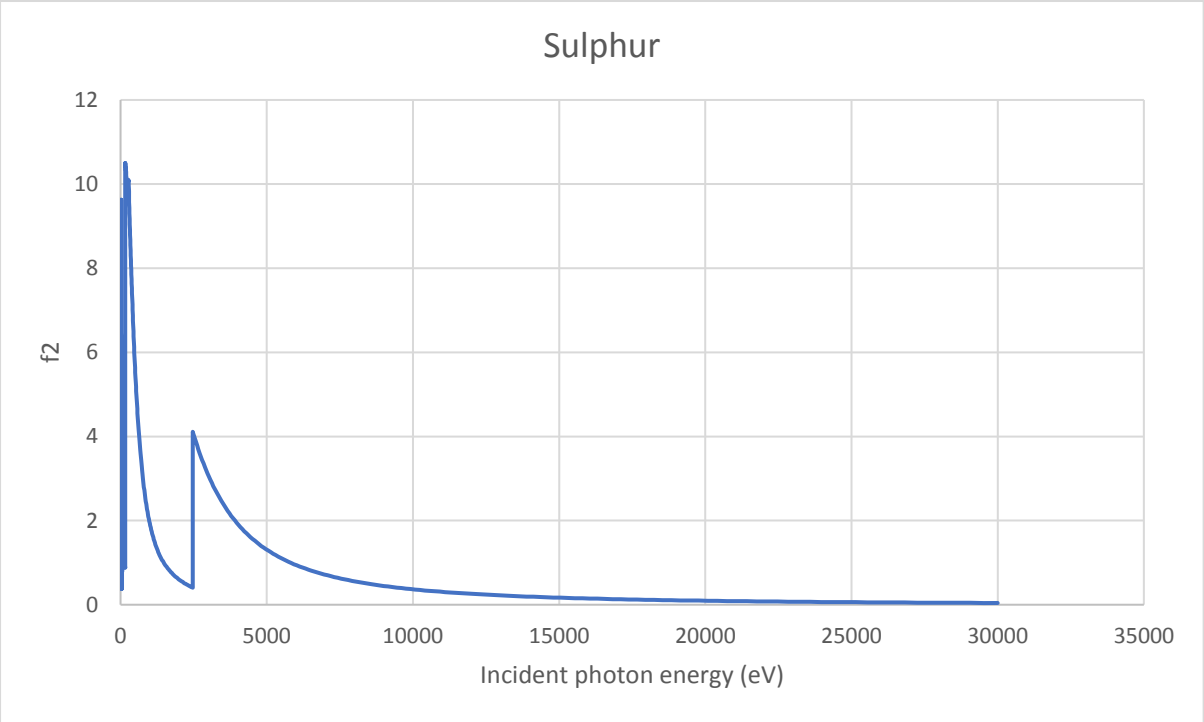

Figure S8 Atomic scattering factor f2 of Sulphur

eV	f_1	f_2	Delta	Beta	$\frac{n_a r_e \lambda^2}{2\pi}$ f1,δ	$\frac{n_a r_e \lambda^2}{2\pi}$ f2,β	% difference	N_a value	% discrepancy
30	1.701	4.838	0.11066	0.31466	0.06505585	0.065039272	0.000254845	8.48E+28	0.091844998
40	2.792	4.725	0.10215	0.17287	0.036586676	0.036586243	1.18304E-05	8.478E+28	0.111609151
60	3.501	6.665	0.056939	0.10839	0.016263639	0.016262566	6.59972E-05	8.48E+28	0.093831708
80	4.833	8.036	0.044206	0.073505	0.0091467	0.009146964	2.88505E-05	8.478E+28	0.111273688
110	6.642	10.25	0.032136	0.049599	0.004838302	0.004838927	0.000129193	8.479E+28	0.103471802
150	10.71	12.13	0.02782	0.031556	0.002597572	0.002601484	0.00150472	8.465E+28	0.270819537
210	15.55	10.85	0.020643	0.014408	0.001327524	0.001327926	0.000302888	8.479E+28	0.10285284
290	18.01	8.649	0.012539	0.006021	0.000696224	0.000696092	0.000190023	8.48E+28	0.08808972
390	19.28	6.72	0.0074216	0.002587	0.000384938	0.000384896	0.000108922	8.48E+28	0.09394614
540	19.48	4.787	0.0039112	0.000961	0.00020078	0.000200762	8.86867E-05	8.479E+28	0.096508022
750	17.58	3.198	0.0018296	0.000333	0.000104073	0.000104071	1.45616E-05	8.479E+28	0.107729417
1000	16.61	16.2	0.0009722	0.000949	5.85322E-05	5.85543E-05	0.000377695	8.477E+28	0.122653493
1420	26.73	10.95	0.000776	0.000318	2.90303E-05	2.90393E-05	0.000308815	8.478E+28	0.114985909
1960	28.81	6.699	0.000439	0.000102	1.52371E-05	1.52381E-05	6.72532E-05	8.478E+28	0.118352815
2700	29.09	3.996	0.0002336	3.21E-05	8.03025E-06	8.02978E-06	5.86755E-05	8.478E+28	0.108456738
3730	28.8	2.329	0.0001212	9.8E-06	4.20833E-06	4.20829E-06	1.10531E-05	8.48E+28	0.092090232
5140	28.34	1.347	6.281E-05	2.98E-06	2.21616E-06	2.21559E-06	0.000257552	8.48E+28	0.092152057
7080	27.65	0.767	3.23E-05	8.96E-07	1.16738E-06	1.1678E-06	0.000358578	8.475E+28	0.149539015
10000	27.71	3.281	1.62E-05	1.92E-06	5.85312E-07	5.85401E-07	0.000151413	8.477E+28	0.124348503

Table S1 Corresponding values of f1, f2, delta and beta at different incident photon energy given by CXRO. n_a was calculated from the constant term $\frac{n_a r_e \lambda^2}{2\pi}$ using values from column $\frac{n_a r_e \lambda^2}{2\pi}$,$f_1$,δ